Sensors & Transducers, Vol. 177, Issue 8, August 2014, pp. 294-301

Sensors & Transducers

Synthetic Sensor of Landsat 7 ETM+ Imagery to Compare and Evaluate Pan-sharpening Methods

Claudio PARENTE and Raffaele SANTAMARIA
Department of Sciences and Technologies, University of Naples "Parthenope"
Directional Centre of Naples, Isle C4, Naples, 80143, Italy
Tel.: 081-5476608, fax: 081-5476514
E-mail: claudio.parente@uniparthenope.it

Received: 22 August 2014 /Accepted: 29 August 2014 /Published: 31 August 2014

Abstract: Several studies and applications are present in literature to compare pan-sharpening methods: the greater part of them is based on indexes that relate radiometric characteristics of derived images to the correspondent original ones. Among others correlation index, RMSE (Root Mean Square Error), UIQI (Universal Image Quality Index) and RASE (Relative Average Spectral Error) are used, but evaluation is limited if there aren't other multispectral images with higher geometric resolution to which compare the pan-sharpened results. In this paper Landsat 7 ETM+ artificial sensor was introduced to permit more reliable comparison and evaluation of pan-sharpening methods. Data concerning Campania region (Italy) were used: firstly Landsat 7 ETM+ panchromatic image and multispectral ones with acquisition bands within that of pan were processed to conduct their digital numbers to radiance values; then synthetic sensor was considered and geometric resolutions degraded by reducing original pixel dimensions 15 m × 15 m and 30 m × 30 m respectively to 30 m × 30 m and 60 m × 60 m. In other terms, new images were derived as equivalent products to those that should have been obtained by sensor with lower geometric resolutions but same acquisition bands of Landsat 7 ETM+ (panchromatic and multispectral). Pan-sharpening methods were applied to derived images and products compared with original data so to obtain a credible evaluation of performances of the implemented approaches.

Keywords: Landsat 7 ETM+ sensor, Pan-sharpening methods, Synthetic sensor, Geometric resolution, Acquisition bands.

1. Introduction

Generally sensors on board of sun-synchronous satellite for remote sensing capture simultaneously images with different spectral and geometric resolutions. Data that are acquired across the visible and most likely also near-infrared wavelengths, so-called panchromatic, present smaller dimensions of pixels and greater width of band relating to others that are named multispectral. If we consider, for example, WorldView-2 imagery, different spatial resolutions are supplied for panchromatic (0.5 m) and multispectral data (2 m): the first are acquired in one band, the second in eight different bands facilitating remote sensing applications, such as land cover classification [1]. Images with spectral resolution of multispectral data and geometric resolution of panchromatic ones are desirable because they permit to have access to more detailed and accurate description of the investigated objects.

Many methods have been developed to get over the limits of the sensors and to produce multispectral images with enhanced spatial resolution using panchromatic data. They are included in data fusion approach and named pan-sharpening methods [2-4].

This paper is aimed to compare some of them using multispectral images with the same geometric resolution of the derived products. In particular Landsat 7 ETM+ sensor was considered: pixels dimensions of the original data were degraded assuming a synthetic sensor and the resulted images submitted to pan-sharpening methods so to verify their performances. High level of likeness between the original (no degraded) images and the pan-sharpened ones showed high level of method effectiveness. The attention was also focalized to evaluate the benefits of bands weights introduction in IHS (Intensity – Hue-Saturation) method as well as in Brovey transformation.

This paper is organized as follows. In Section 2 short report of the main characteristics of Landsat 7 ETM+ sensor and imagery is supplied together with the description of the first elaborations of data concerning Campania region (Italy). Section 3 is focalized on the application of some selected pan-sharpening methods of which fundamental characteristics are summarized. For analytical evaluation of the results, quality indexes are shown and discussed in Section 4. Considerations about the adopted solutions and conclusions are reported in Section 5.

2. Data and First Elaborations

2.1. Landsat 7 ETM+ Images

The Landsat Program is a joint effort of the U.S. Geological Survey (USGS) and the National Aeronautics and Space Administration (NASA) for Earth Observation; it represents the world's longest running system of satellites for moderate-resolution optical remote sensing for land, coastal areas and shallow waters [5].

Landsat 7 satellite was launched on April 15, 1999, and is still operational. It makes a complete orbit around the Earth every 99 minutes moving in descending way (from north to south), over the sunlit side of the planet, at 705 kilometers (438 miles) altitude. This satellite completes about 14 full orbits each day and crosses every point on Earth once every 16 days; swath is 185 kilometers [6].

This satellite carries the sensor named Enhanced Thematic Mapper Plus (ETM+), with spatial resolution of 30 m for visible, NIR (near infrared), and SWIR (shortwave infrared) bands, 60 m for thermal band, and 15 m for panchromatic band. Wavelengths range and cell size for each band are reported in Table 1.

For this application Landsat 7 ETM+ imagery of Campania region (Italy) by USGS were considered (Fig. 1). Data were already radiometrically and geographically corrected, but fitted in 8 bit files (ranges from 0 to 255).

Table 1. Landsat 7 ETM+ bands and geometric resolutions (Source: Chander et al, 2009).

Spectral Band	Actual Wavelengths (micrometers)	Geometric resolution (meters)
Band 1	0.452-0.514	30
Band 2	0.519-0.601	30
Band 3	0.631-0.692	30
Band 4	0.772-0.898	30
Band 5	1.547-1.748	30
Band 6	10.31-12.36	60
Band 7	2.065-2.346	30
Band 8	0.515-0.896	15

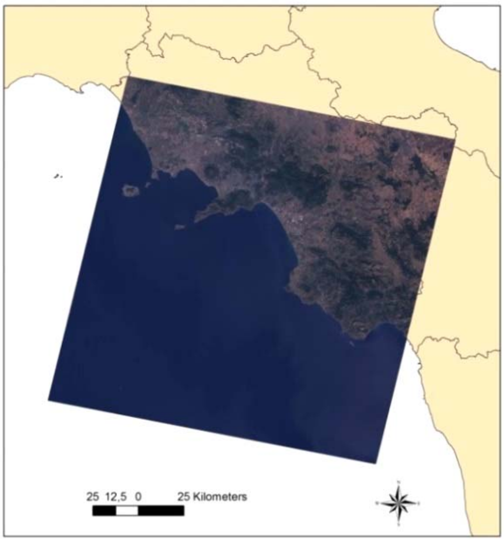

Fig. 1. RGB composition (Bands 3, 2, 1) of the original Landsat 7 ETM+ imagery in overlay with administrative boundaries of Italian Regions.

2.2. Radiance Calculation

To generate results of synthetic sensor (SynS), calculation of at-sensor spectral radiance, also called top-of-atmosphere radiance, occurred. In fact each image was matrix of DNs (Digital Numbers) and to transform them in radiance values, the following formula [7-9] was applied:

$$L_\lambda = gain_\lambda \cdot DN + bias_\lambda, \tag{1}$$

where L_λ is the calculated radiance associated to the ground area enclosed in the pixel and referred to the λ wavelength range of the specific band; *DN* is the digital number of the pixel of the Landsat 7 ETM+ band image; $gain_\lambda$ (W/(m^2 sr μm DN) and $bias_\lambda$ (W/(m^2 sr μm)) are sensor-specific calibration parameters determined for each band before the launch.

To maximize the sensor 8-bit radiometric resolution without saturating the detectors, the acquisition of ETM+ images is in either a low- or high-gain way: the first mode is used to image surfaces with high brightness (higher dynamic range but low sensitivity); the second mode is used to image surfaces with low brightness (lower dynamic range but high sensitivity) [10].

Gain and bias values for Landsat 7 ETM+ bands are reported in Table 2 (low-gain mode) and Table 3 (high- gain mode).

Table 2. Gain and bias values for Landsat 7 ETM+ bands - low-gain mode (Source: Chander et al, 2009).

Spectral Band	Gain W/(m^2 sr μm DN)	Bias W/(m^2 sr μm)
Band 1	1.180709	−7.38
Band 2	1.209843	−7.61
Band 3	0.942520	−5.94
Band 4	0.969291	−6.07
Band 5	0.191220	−1.19
Band 6	0.067087	−0.07
Band 7	0.066496	−0.42
Band 8	0.975591	−5.68

Table 3. Gain and bias values for Landsat 7 ETM+ bands - high-gain mode (Source: Chander et al, 2009).

Spectral Band	Gain W/(m^2 sr μm DN)	Bias W/(m^2 sr μm)
Band 1	0.778740	−6.98
Band 2	0.798819	−7.20
Band 3	0.621654	-5.62
Band 4	0.639764	-5.74
Band 5	0.126220	−1.13
Band 6	0.037205	3.16
Band 7	0.043898	−0.39
Band 8	0.641732	−5.34

Formula (1) was applied to panchromatic image (band 8) and those multispectral images which acquisition bands are within that of pan (bands 2, 3 and 4); in other terms, only data to be used for pan-sharpening methods application were considered.

2.3. Degradation of Geometric Resolutions and Generation of New DNs Matrices

To simulate acquisition by SynS with the same considered spectral bands of Landsat 7 ETM+ but lower geometric resolutions, the original matrices of radiance were resampled from 30 m to 60 m for bands 2, 3, 4, and from 15 m to 30 m for band 8. In every case, each group of 4 pixels was substituted by one cell: radiance value was derived by correspondent four primary ones as average. Then matrices of DNs were obtained from those resampled matrices of radiance using the inverse of formula (1):

$$DN = \frac{L_\lambda - bias_\lambda}{gain_\lambda}, \qquad (2)$$

In this way 4 new images (bands 2, 3, 4 and 8) were achieved as those that should have been captured by another sensor (SynS) in the same position of ETM+ at the same acquisition instant, but with lower geometric resolutions.

3. Applications of Pan-sharpening Methods

A clip was extracted from dataset by SynS as illustrated in Fig. 2 before to continue the experimentation. To produce fusion between panchromatic, with higher spatial resolution, and multispectral data, characterized by higher spectral resolution but less spatial detail, the following pan-sharpening methods were applied.

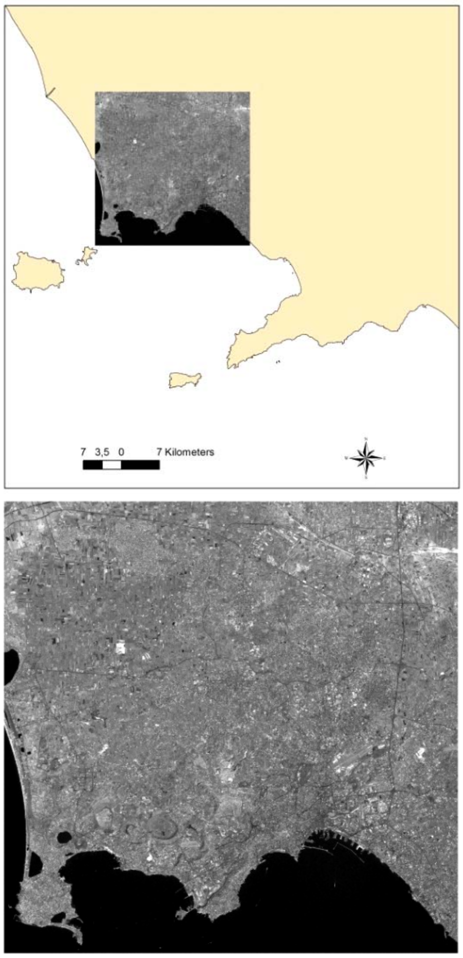

Fig. 2. Clip of dataset to which pan-sharpened methods were applied: localization (upper) and visualization of panchromatic layer (lower).

Multiplicative method [11]. The pan-sharpened image is obtained with the formula:

$$psh_i = \frac{Pan}{\mu_{Pan}} \cdot Mul_i, \qquad (3)$$

where psh_i is the pan-sharpened ith image; *Pan* is the panchromatic image; Mul_i is the multispectral ith image; μ_{Pan} is the mean of panchromatic image.

Simple Mean method. This method applies a simple mean averaging equation to each combination of Pan with one of multispectral images [12]. For consequence the pan-sharpened image is obtained with the formula:

$$psh_i = \frac{Pan + Mul_i}{2}, \tag{4}$$

IHS method [13-15]. It is based on RGB (Red-Green-Blue) to IHS (Intensity-Hue-Saturation) space transformation. The intensity component *I* is substituted by the panchromatic image because of their similarity and the inverse transformation (from IHS to RGB space) is applied. R' G' B' components with the same geometric resolution of panchromatic data are produced using the following equation:

$$\begin{bmatrix} R' \\ G' \\ B' \end{bmatrix} == \begin{bmatrix} R+\delta \\ G+\delta \\ B+\delta \end{bmatrix}, \tag{5}$$

where

$$\delta = Pan - I, \tag{6}$$

To calculate *I*, the following formula is used:

$$I = \frac{R+G+B}{3}, \tag{7}$$

In the case of Landsat 7 ETM+ as well as SynS, considering the acquisition bands, *I* can be obtained as simple mean of bands 2, 3 and 4 (respectively indicated as B_2, B_3, B_4):

$$I = \frac{B_2 + B_3 + B_4}{3}, \tag{8}$$

In alternative different weights can be given to each multispectral image:

$$I = \frac{a \cdot B_2 + b \cdot B_3 + c \cdot B_4}{a+b+c}, \tag{9}$$

where a, b and c are the weights assigned to the bands 2, 3 and 4, respectively.

According to the approach that was adopted in a previous work for Quickbird images [16], also for Landsat 7 ETM+ and consequently for SynS the values of these parameters were estimated considering the relative spectral response (RSR) in Fig. 3. Calculating the contribution of each multispectral band in percentage to the sum of the contributions of all multispectral bands to panchromatic one, the weights in Table 4 were obtained.

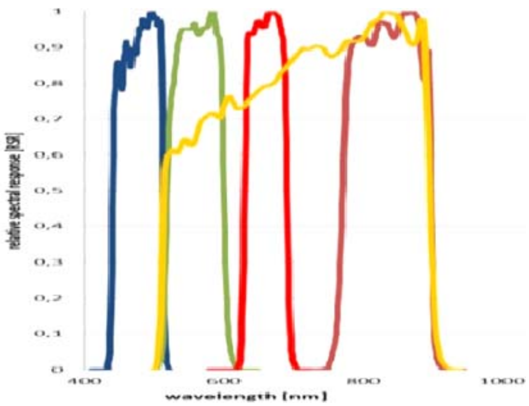

Fig. 3. Relative spectral response (RSR) of Landsat 7 ETM+ (bands 1, 2, 3, 4, 8).

Table 4. Values of weights for multispectral images derived by RSR.

	Band 2	Band 3	Band 4
Weights	0.26	0.22	0.52

Brovey transformation [17, 18]. With this method each pan-sharpened image is obtained by *n* multispectral bands using the formula:

$$psh_i = \frac{Pan}{\frac{\sum_{i=1}^{n} Mul_i}{n}} \cdot Mul_i, \tag{10}$$

Also in this case weights can be introduced for the multispectral bands and the formula becomes:

$$psh_i = \frac{Pan}{\frac{\sum_{i=1}^{n} p_i Mul_i}{\sum_{i=1}^{n} p_i}} \cdot Mul_i, \tag{11}$$

Of course in this application the same weights reported in Table 4 for multispectral SynS images were adopted in the case of Brovey transformation.

In Fig. 4 RGB compositions with original synthetic images as well as pan-sharpened ones from each considered method are reported. Even if false color (bands 3, 2, 4), they permitted the first evaluation of results: multiplicative and simple mean methods produced greater color distortion than IHS and Brovey transformation; these effects are reduced with bands weights introduction.

Quantitative analysis of the performance of each method was conducted by checking usual protocols that are present in literature. Particularly the following indexes that compare statistic characteristics of input and output images were considered.

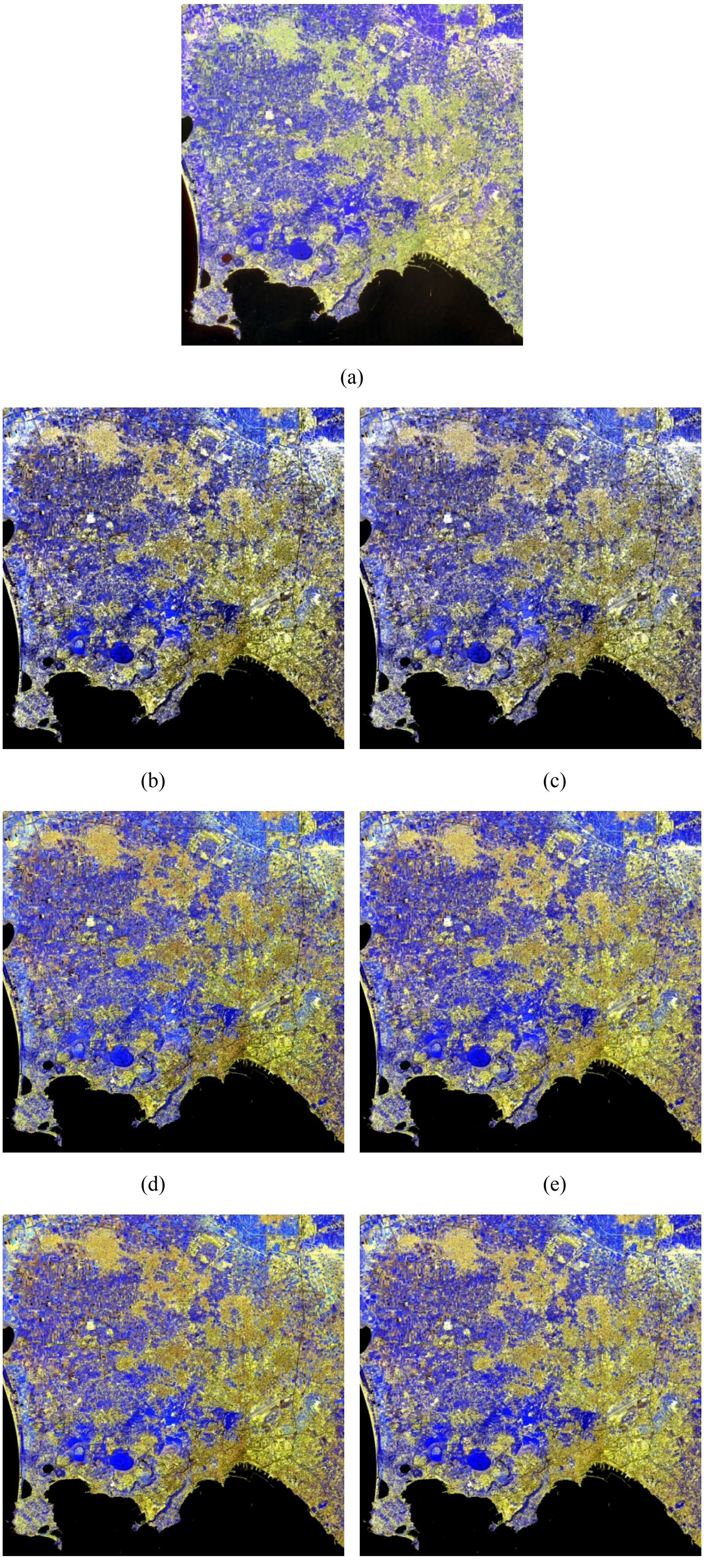

(a)

(b) (c)

(d) (e)

(f) (g)

Fig. 4. RGB false color compositions (bands 3, 2, 4) with SynS multispectral images (a) and pan-sharpened images by methods: Multiplicative (b), Simple mean (c), IHS (d), IHS with bands weights (e), Brovey transformation (f), Brovey transformations with bands weights (g).

4. Results and Discussion

Correlation Coefficient (ρ). It is the most used measurement of spatial fidelity and supplied by the formula:

$$\rho_{AB} = \frac{Cov_{AB}}{\sigma_A \cdot \sigma_B}, \qquad (12)$$

where A is the input multispectral image; B is the correspondent output multispectral image; σ_A is standard deviation of image A; σ_B is standard deviation of image B; Cov_{AB} is covariance between A and B.

Universal Image Quality Index (UIQI). Introduced by Wang and Bovik (2002) [19], this index can be calculated as:

$$UIQI_{AB} = \frac{Cov_{AB}}{\sigma_A \sigma_B} \cdot \frac{2\mu_A \mu_B}{\mu_A^2 + \mu_B^2} \cdot \frac{2\sigma_A \sigma_B}{\sigma_A^2 + \sigma_B^2}, \qquad (13)$$

where μ_A is the mean value of image A; μ_B is the mean value of image B.

Root mean square error (RMSE). It is computed using the formula [20]:

$$RMSE_{AB} = \sqrt{BIAS_{AB}^2 + \sigma_{AB}^2}, \qquad (14)$$

where $BIAS_{AB}$ is the difference between the mean values of the input multispectral image and the output one; σ_{AB} is standard deviation of difference image A-B.

Relative average spectral error (RASE). This index is calculated including all multispectral images [21]:

$$RASE = \frac{100}{M} \sqrt{\frac{1}{n} \sum_{i=1}^{n} RMSE_i^2}, \qquad (15)$$

where M is the mean value of DNs of the n input images.

Tables 5-10 give values of the above mentioned indexes for each method.

All indexes confirmed that better results were supplied by IHS method and Brovey transformation, both with bands weights introduction. Nevertheless, in spite of color distortions that were evident in visual comparisons, in many cases values of indexes resulted very good, with low differences between one method and another. Considering, for example, UIQI average for Simple mean method (about 95 %), pan-sharpened images should have been characterized by high quality, but this was not true. On the other side, comparison of values for each index permitted to obtain the same classification; particularly better results are confirmed for IHS method with bands weights and Brovey transformation with bands weights.

Table 5. Values of quality indexes for Multiplicative method.

	ρ	*UIQI*	*RMSE*	*RASE*
Band 2	0.957	0.944	25.726	
Band 3	0.959	0.947	25,525	
Band 4	0.949	0.943	24.437	
	0.955	0.944	25.229	20.608

Table 6. Values of quality indexes for Simple mean method.

	ρ	*UIQI*	*RMSE*	*RASE*
Band 2	0.943	0.942	22.435	
Band 3	0.937	0.934	21.445	
Band 4	0.975	0.975	21.323	
	0.952	0.950	21.734	17.753

Table 7. Values of quality indexes for IHS method.

	ρ	*UIQI*	*RMSE*	*RASE*
Band 2	0.915	0.914	26.931	
Band 3	0.919	0.917	27.182	
Band 4	0.959	0.959	18.126	
	0.931	0.930	24.080	19.963

Table 8. Values of quality indexes for IHS method with bands weights.

	ρ	*UIQI*	*RMSE*	*RASE*
Band 2	0.958	0.957	19.422	
Band 3	0.960	0.957	19.924	
Band 4	0.970	0.970	15.572	
	0.963	0.961	18.306	15.033

Table 9. Values of quality indexes for Brovey transformation.

	ρ	*UIQI*	*RMSE*	*RASE*
Band 2	0.925	0.924	25.068	
Band 3	0.935	0.935	23.827	
Band 4	0.949	0.941	25.288	
	0.936	0.933	24.728	20.200

Table 10. Values of quality indexes for Brovey transformation with bands weights.

	ρ	*UIQI*	*RMSE*	*RASE*
Band 2	0.956	0.955	19.478	
Band 3	0.960	0.960	19.041	
Band 4	0.971	0.969	17.149	
	0.962	0.961	18.556	15.176

Analysis was perfected using original multispectral images: the performance of each method was evaluated comparing to them pan-sharpened datasets. Table 11 gives values of RMSE for all considered methods.

In this case the previous classification of performances, obtained with quality indexes of comparison between resampled and pan-sharpened images, was confirmed. However range of values was greater, so differences could be better detected: results of IHS method with weights and Brovey transformation with weights were similar in the first analysis while they became more distant in the second case.

Table 11. Values of RMSE for considered pan-sharpened methods.

Method	Band 2	Band 3	Band 4	Average
Multip.	33.364	34.956	24.803	31.041
Simp. M.	26.673	28.284	16.584	23.847
IHS	27.462	27.876	18.360	24.566
IHS+W	21.599	22.324	15.347	19.757
Brovey	26.553	26.801	25.734	26.363
Brovey+W	23.648	25.191	17.155	21.998

The best performance of IHS confirms that it is the most straightforward fusion method when the multispectral bands are exactly three [22, 23].

5. Conclusions

Possibility to use high resolution multispectral images permits to conduct more reliable comparison and evaluation of pan-sharpening methods. The use of dataset by different sensor on different satellite and probably with different acquisition date presents new variables and complications.

This study proposed an alternative approach: to introduce synthetic sensor for production of degraded images and apply to them the different methods to be evaluated. In this case to pass from DNs to at-sensor spectral radiance is necessary: it is possible to assume that the new sensor intercepts the same energy like the real sensor, but with different spatial resolutions. The equation to pass from DNs to radiance for Landsat 7 ETM+ is well known in literature, so it is easy to be applied.

The results confirm higher performances of IHS method and Brovey transformation when weights are introduced to distinguish the different rule of each multispectral acquisition band in pan-sharpening operations.

The approach as proposed cannot be applied to establish every time in real applications which pan-sharpened images are better than others, but supplies possibility to classify performance of each method. For consequence it can be used also to test new algorithms and procedures.

In this application transformations to halve pixel dimensions were considered, but also cases with more reductions of cell sizes for pan-sharpened images must be analyzed; in this way to establish performance of each method in reference to increasing levels of geometric resolution will be possible.

References

[1]. P. Maglione, C. Parente, R. Santamaria, A. Vallario, Modelli tematici 3D della copertura del suolo a partire da DTM e immagini telerilevate ad alta risoluzione WorldView-2, *Rendiconti Online Della Società Geologica Italiana*, Vol. 30, 2014, pp. 33-40 (in Italian)

[2]. B. Aiazzi, S. Baronti, F. Lotti, M. Selva, A comparison between global and context-adaptive pansharpening of multispectral images, *IEEE Geoscience and Remote Sensing Letters*, Vol. 6, Issue 2, 2009, pp. 302–306.

[3]. Y. Zhang, Understanding image fusion, *Photogrammetric Engineering & Remote Sensing*, Vol. 70, Issue 6, 2004, pp. 657-671.

[4]. I. Amro, J. Mateos, M. Vega, R. Molina, A. K. Katsaggelos, A survey of classical methods and new trends in pansharpening of multispectral images, *EURASIP Journal on Advances in Signal Processing,* Springer Open Journal, Vol. 79, 2011, (http://asp.eurasipjournals.com/content/2011/1/79).

[5]. ESRIN. IDEAS – LANDSAT products description document, *IDEAS-VEG-SRV-REP-1320*, Issue 3, 06 June 2014, Telespazio VEGA UK Ltd, (http://www.telespazio-vega.com).

[6]. Landsat – A global land-imaging mission, *US Geological Survey*, (http://usgs.gov/fs/2012/3072/fs2012-3072.pdf).

[7]. G. J. Firl, L. Carter, Lesson 10: Calculating vegetation indices from Landsat 5 TM and Landsat 7 ETM+ Data, *Colorado State University*, (http://ibis.colostate.edu/WebContent/WS/ColoradoView/TutorialsDownloads/CO_RS_Tutorial10.pdf.

[8]. X. Chen, L. Vierling, D. Deering, Simple and effective radiometric correction method to improve landscape change detection across sensors and across time, *Remote Sensing of Environment*, Vol. 98, 2005, pp. 63-79.

[9]. S. C. Goslee, Analyzing remote sensing data in R: The Landsat Package, *Journal of Statistical Software*, Vol. 43, Issue 4, 2011, pp. 1-25.

[10]. G. Chander, B. L. Markham, D. L. Helder, Summary of current radiometric calibration coefficients for Landsat MSS, TM, ETM+, and EO-1 ALI sensors, *Remote Sensing of Environment*, Vol. 113, 2009, pp. 893-903.

[11]. Q. Du, N. H. Younan, R. King, V. P. Shah, On the performance evaluation of pan-sharpening techniques, *IEEE Geoscience and Remote Sensing Letters*, Vol. 4, Issue 4, October 2007, pp. 518-522.

[12]. ArcGIS 9.3 Desktop Help, *ESRI (Environmental Systems Research Institute)*, USA, 2008.

[13]. M. Basile Giannini, P. Maglione, C. Parente, Application of IHS Pan-Sharpening techniques to IKONOS images, in *Proceedings of the IEEE GOLD Conference 2010*, Livorno, Italia, April 29-30, 2010, (http://ieee.uniparthenope.it/chapter/_private/proc10/24.pdf).

[14]. Y. Ling, M. Ehlers, E. L. Usery, M. Madden, FFT enhanced IHS transform method for fusing high resolution satellite images, *ISPRS Journal of Photogrammetry and Remote Sensing*, Vol. 61, 2007, pp. 381-392.

[15]. T. M. Tu, P. Huang, C. L. Hung, C. P. Pang, A fast Intensity – Hue – Saturation fusion technique with spectral adjustment for IKONOS imagery, *IEEE Geoscience and Remote Sensing Letters*, Vol. 1, Issue 4, 2004, pp. 309-312.

[16]. C. Parente, R. Santamaria, Increasing geometric resolution of data supplied by quickbird multispectral sensors, *Sensors & Transducers,* Vol. 156, Issue 9, September 2013, pp. 111-115.

[17]. R. J. Vrabel, Multi-spectral imagery advanced band sharpening study, *Photogrammetric Engineering and Remote Sensing*, Vol. 66, Issue 1, 2006, pp. 73-79.

[18]. K. G. Nikolakopoulos, Comparison of nine fusion techniques for very high resolution data, *Photogrammetric Engineering & Remote Sensing*, Vol. 74, Issue 5, May 2008, pp. 647-659.

[19]. Z. Wang, A. C. Bovik, A universal image quality index, *IEEE Signal Processing Letters,* Vol. 9, Issue 3, 2002, pp. 81–84.

[20]. S. Chen, R. Zhang, H. Su, J. Tian, J. Xia, Scaling-up transformation of multisensor images with multiple resolutions, *Sensors*, Issue 9, 2009, pp. 1370-1381.

[21]. L. Wald, Quality of high resolution synthesized images: Is there a simple criterion? in *Proceedings of the International Conference Fusion of Earth Data*, January 26-28, 2000, Nice, France, 2000, Vol. 1, pp. 99-105.

[22]. W. Carper, T. Lillesand, R. Kiefer, The use of intensity-hue-saturation transformations for merging SPOT panchromatic and multispectral image data, *Photogrammetric Engineering & Remote Sensing*, Vol. 56, Issue 4, 1990, pp. 459-467.

[23]. B. Aiazzi, L. Alparone, S. Baronti, A. Garzelli, M. Selva, MTF-tailored multiscale fusion of high-resolution MS and Pan imagery, *Photogrammetric Engineering & Remote Sensing*, Vol. 72, Issue 5, 2006, pp. 591-596.
